Influence of Polymer Structure upon Active-Ingredient Loading: a Monte Carlo Simulation Study for Design of Drug-Delivery Devices

Alberto Striolo[#], Dusan Bratko, John M. Prausnitz[*]

Chemical Engineering Department
University of California, Berkeley
and
Chemical Sciences Division
Lawrence Berkeley National Laboratory
Berkeley, CA 94720

and

Nicola Elvassore and Alberto Bertucco

Istituto di Impianti Chimici
Università di Padova, Via Marzolo 9, I-35131 Padova, Italy

[#] Speaker

* to whom correspondence should be addressed

Abstract

Drug -loaded polymers and polymeric microparticles provide an attractive form for controlled drug-delivery systems. Design of new systems requires knowledge of polymer-drug interactions. The effect of polymer architecture and chemistry upon active-ingredient loading is investigated by Monte Carlo simulation. The ensemble-growth method is used to sample conformations of a model polymer comprising polar and nonpolar segments. The polymer is a block copolymer, linear or branched. In our calculations, the polar portion of the polymer contained 21 segments. The polymers are dissolved in either of two types of solvent models. In the first, nonpolar solvent, the polar segments tend to collapse, but the bulky nonpolar groups, easily soluble in the medium, create some cavities in the polymer. These cavities are suitable hosts for the slightly polar active ingredient. In the second solvent, polar, the nonpolar segments contribute to attract the active ingredient within the polymer segments, therefore lowering the burst-release rate. The relative uptake of the active ingredient, proportional to the probability of finding an active ingredient within the radius of gyration of the polymer, is computed as a function of the number of nonpolar segments in the polymer. Simulation results are reported for active ingredients of two different sizes. For given size of the polar portion, short nonpolar tails increase the active-ingredient relative uptake in both solvents considered. Linear block copolymers look promising for obtaining higher entrapment efficiency for the active ingredient and for controlled release.

Key words: Drug Delivery, Monte Carlo Molecular Simulation, Ensemble-Growth

Introduction

Microencapsulation is a widely utilized vehicle for controlled delivery of active ingredients and for other applications [1]. This technique is often used to enhance and prolong the effectiveness of active ingredients (proteins, flavors, anesthetics …) [2-5], to enhance the adhesion of the microparticle to a targeted site or to control the active-ingredient release rate [6, 7]. Different techniques are available to trap an active ingredient into a polymeric microparticle [1]: classical methods use spray drying [8], emulsions or double-emulsions water/oil/water (w/o/w), or solvent evaporation [9]. New methods are based on supercritical fluids such as aerosol solvent extraction systems (ASES) [10] or supercritical anti-solvent methods [11].

The physical entrapment of an active ingredient into a polymeric material can be thermodynamically unfavorable. In this case, the entrapment can be controlled kinetically; for example, in the production of drug-containing polymer particles by precipitation with supercritical CO_2, the pharmaceutical does not have enough time to 'escape' from the polymeric matrix before it is trapped at supersaturation conditions [11]. Improving the polymer-active ingredient affinity may lead to higher entrapment ratios [12].

Numerous drugs are partially hydrophilic and some genetic-therapy agents, such as DNA molecules, present extremely hydrophilic characteristics. The polarities of these molecules could lead to low entrapment efficiencies and high initial burst-release rates [8]. Different polymers are under development to achieve a target-delivery system [13] or to improve the active-ingredient loading per particle [12]. Copolymers are promising for pharmaceutical applications [5, 12]. Because copolymers are chemically heterogeneous, they may enhance the entrapment efficiency and lower the initial burst-release rate.

Recently, dendrimers [14] containing a hydrophilic backbone, partially hydrophobic intermediate shells and highly hydrophobic chain ends have been synthesized [15]. In a hydrophobic environment, the internal hydrophilic core is collapsed and the hydrophobic shells assure solubility. In a hydrophilic environment, the core, if big enough, wraps the hydrophobic tails, exposing itself to the solvent [15]. This system appears promising for a delivery system for polar active ingredients; in a nonpolar environment, typical for microcapsules production, the polar active ingredient is attracted by the polymeric internal core, followed by release upon immersion in polar solvents (e.g. human blood). However, dendrimers may present high segment density near the center of mass [16]. Therefore, the active-ingredient entrapment may be difficult due to steric effects. In this case, linear block copolymers containing three chemically different types of segments may improve the active-ingredient entrapment ratio.

Due to the wide variety of polymer-active ingredient combinations, experimental determination of delivery systems for a particular drug requires expensive and time-consuming trial-and-error procedures [2]. Goddard and coworkers [17] showed that molecular simulation techniques can assist in designing polymeric systems for encapsulation of specified molecules. Using Monte Carlo molecular simulations, this study investigates potential application of block copolymers, both linear and dendrimer-like, as matrices for the production of active-ingredient-containing microparticles. Our goal is to reduce and to guide necessary experimental work.

Simulation Method

The polymer is represented by a sequence of freely-jointed-tangent-hard-sphere segments. Figure 1 shows the polymer architectures considered here. The linear block copolymer (LBC) (Figure 1a) contains three sequences of segments: polar segments (type-A segments), partially nonpolar segments (type B) and nonpolar segments (type C). Similar polymer segments are used for dendrimer-like copolymers for which the core is built with segments of type A, the 'intermediate' shell with type-B segments and the 'external' shell with type-C segments. Figure 1b shows a branched polymer with a linear core (DENDL) and Figure 1c shows a branched polymer with a 4-arm star core (DENDS). The size of the polar section is kept equal to 21 segments in each computer experiment. To simulate a dilute solution, only one active ingredient was considered per polymer molecule. The active ingredient is represented by a hard sphere. Steric exclusion is likely to play a major role in active-ingredient loading. The tangent-hard-sphere model is therefore preferred over a ball-and-stick model to secure a more realistic account of excluded-volume effects. This model also facilitates a coherent way to represent both polymer segments and active-ingredient molecules. Dynamic Monte Carlo techniques such as the reptation algorithm [18, 19] are not used here because they are inefficient when simulating heteropolymers and branched polymers [20]. We use a non-dynamic ensemble-growth algorithm. This method is well described elsewhere [21, 22] and is widely used to study a single polymer molecule. In this work, we apply a generalization of that method to many-body systems [23] to consider polymer-active ingredient equilibria.

The algorithm builds simultaneously, step by step, an ensemble of M_c polymer-active ingredient couples. The first two segments of the M_c molecules are introduced at the

starting step of the simulation. For each of the M_c molecules in the ensemble, five possible positions of the third segments are randomly chosen around the second ones. Among the total $5\times M_c$ possibilities, M_c molecules belonging to the ensemble are randomly chosen according to Boltzmann probability. In the next step, the fourth segments are attached in the same way as that for the third ones. The procedure is repeated until the polymer is completed. The algorithm builds the polymer in the following order: core, intermediate, and external shell for branched polymers; first, second, and third block for linear copolymers.

The active ingredient is the last, non attached unit in the system. To obtain the active-ingredient radial distribution function as a function of the distance from the center of mass of the polymer, each polymer is placed in a cubic box of size equal to eight times the radius of gyration of the polymer. Ten possible positions of the active ingredient are randomly chosen in the box for a total of $10\times M_c$ replicas of the polymer-active ingredient pair. Among these, M_c couples are randomly chosen according to Boltzmann probability and retained in the ensemble. Since the active ingredient is modeled as a single sphere, the same batch of M_c polymers is used to obtain at least $200\times M_c$ polymer-active ingredient pairs.

In the present work, the ensemble contains M_c=5,000 polymer-active ingredient couples. To verify statistical accuracy, one case with M_c=10,000 couples was run for each situation tested. No significant difference in the active ingredient radial distribution function was observed. The results reported here represent the average of a total of four different runs for each situation.

Because the medium is considered as a continuum, phenomena determined by solvent molecules, such as hydrogen bonding, are not explicitly considered at a molecular level. For effective interactions we use potentials of mean force that correspond to the canonical average over all solvent configurations. The McMillan-Mayer level of description [24] can describe the equilibrium properties of dilute polymer solutions [25]. The solvent-mediated segment-segment and segment/active-ingredient interactions are represented by a square-well potential whose well depth depends on the species considered. Well width is held equal to the radius of a segment. The square-well potential, ϕ_{ii}, is a function of the distance *d* between segments according to:

$$\phi_{ii}(d) = \begin{cases} \infty & for \quad 0 < d < \sigma_{ii} \\ -\varepsilon & for \quad \sigma_{ii} < d < 1.5 \cdot \sigma_{ii} \\ 0 & for \quad 1.5 \cdot \sigma_{ii} < d \end{cases}, \tag{1}$$

where σ_{ii} and ε are the hard-sphere diameter and well depth. Interaction parameters between unlike species are obtained from the parameters between like species according to conventional combining rules:

$$\varepsilon_{ij} = \sqrt{\varepsilon_{ii} \cdot \varepsilon_{jj}} \quad , \tag{2}$$

$$\sigma_{ij} = \frac{1}{2} \cdot (\sigma_i + \sigma_j) \quad , \tag{3}$$

The subscripts refer to different segments and/or active ingredient. Polymer segment diameters are chosen such that they reproduce the size parameters for a square-well equation of state for the different kinds of monomer considered in this work [26]. Type-A segments are polar, similar to polyethylene oxide segments; the diameter of one of its segments is considered as the unit length. Type-B segments are partially nonpolar, similar to polystyrene segments, while type-C segments are slightly bigger and nonpolar. The

diameters chosen to represent the active ingredient correspond to molecular weights between 150 and 300 g/mol.

The pure-component well depths are arbitrarily chosen such that they roughly reproduce segment-segment interactions in either polar or nonpolar solvents. Theta conditions [27] for a square-well chain correspond to a well depth –0.32 k_BT when the well width equals the segment radius [28]. In nonpolar environments, the polar segments are at poor-solvent conditions (well-depth above 0.32 k_BT) while the nonpolar segments are at good-solvent conditions (well-depth below 0.32 k_BT). The opposite applies in polar solvents. Active ingredients of two different sizes are considered. Both active ingredients are considered partially polar.

The active ingredient relative uptake, AI_{ru} is here defined as:

$$AI_{ru} = \frac{\int_0^{R_g} \rho(r) \cdot r^2 dr}{\frac{1}{3} \cdot \langle \rho \rangle \cdot R_g^3} \quad , \qquad (4)$$

where $<\rho>$ is the average active-ingredient density in the simulation box, $g(r)$ is the active-ingredient radial distribution function as a function of distance from the center of mass of the polymer, $\rho(r)$ is the active-ingredient local density ($=<\rho>g(r)$), and R_g is the square root of the sample average radius of gyration squared, computed in the absence of active ingredient. In Equation 4 the numerator is the probability of finding one active ingredient molecule within the polymer, while the denominator is the probability of finding an active ingredient molecule in an equal volume of solution far from the polymer [29]. When AI_{ru} is higher than unity, the active ingredient is attracted within the polymer segments, while when it is less than unity, the active ingredient is repelled from the

polymer segments into the bulk solution. The higher the value AI_{ru}, the more probable the active ingredient is entrapped into the polymeric matrix.

Results and Discussion

Table 1 shows energy and size parameters used to represent different solvent conditions. The active ingredient is trapped in the polymeric matrix at nonpolar solvent conditions. Table 2 shows the results obtained for AI_{ru} for both active ingredients at nonpolar-solvent conditions, together with the sample average radii of gyration squared of the polymers. The sample average radii of gyration squared are reduced by the diameter of a type-A segment. To enhance the active ingredient uptake at nonpolar solvent conditions, AI_{ru} should be higher than unity. For all the polymer architectures considered, increasing the number of nonpolar segments increases AI_{ru}. The results obtained for AI1 with LBC and DENDL polymers are similar, although AI_{ru} is generally higher for LBC than for DENDL polymers. For AI2, only LBC and DENDL polymers are considered. For both active ingredients in solution with DENDS polymers, adding a few nonpolar segments increases AI_{ru} more than 100%, while with LBC polymers, the increase is only about 20%. For a given number of segments, AI_{ru} with LBC is higher than that for DENDS polymers. In particular, AI_{ru} for DENDS is lower than unity when the nonpolar segments are only a few, indicating that this polymer architecture is not suitable for production of active-ingredient-loaded microparticles. This unsuitability is probably due to the high segment density around the center of mass of the polymer: a branched polymer (like DENDS) does not contain many cavities for harboring an active ingredient. These results agree with measurements of distribution coefficients of hydrophobic substrates via electrokinetic chromatography using dendrimers of different generations as pseudostationary phase [30].

The distribution coefficient was defined as the substrate concentration associated with the pseudostationary phase divided by the substrate concentration in the mobile phase. For a given substrate, the reported distribution coefficient decreases with increasing dendrimer generation number from one to three. This shows that the dendrimer-substrate affinity decreases with increasing polymer degree of branching.

Figure 2 shows the segment density as a function of distance from the center of mass of the polymer. The polymer is dissolved at nonpolar-solvent conditions. The segment density is reported upon completion of the core, of the intermediate shell, and of the external shell for a DENDS polymer with 21 type-A segments, 4 type-B and 8 type-C segments. The presence of nonpolar tails produces reduced segment density around the center of mass, increasing the radius of gyration of the polymer, and also increasing the number of vacancies between polymer segments. This effect enhances the uptake of partially polar active ingredients. The effect of polymer architecture upon active-ingredient uptake is more pronounced for the larger active ingredient.

Figures 3 and 4 show the radial distribution functions of AI2 as a function of distance from the center of mass of the polymer in solutions with LBC and DENDS polymers, respectively. The distance is reduced by the radius of gyration of the polymer. In both figures, increasing the number of hydrophobic segments gives rise to an increase of the radial distribution function at low distances from the center of mass; this increase improves the active ingredient uptake. Figure 4 shows that the active ingredient does not find suitable cavities within the branched polymer, unless the nonpolar tails are quite long. However, in any case, the active ingredient can be found at distances that are lower than half the radius of gyration from the center of mass of the polymer.

The active ingredient is released from the particle in a polar environment where the nonpolar segments are at poor solvent conditions and the polar segments are at good solvent conditions. Table 3 shows the results obtained for both active ingredients AI_{ru} at polar-solvent conditions. To release the active ingredient from the polymeric matrix, AI_{ru} should be less than unity, but to avoid a burst release, AI_{ru} should not be close to zero. The few results obtained suggest that linear copolymers made by a few nonpolar segments are probably suitable for controlled release of the active ingredient. It appears that the larger active ingredient is released more rapidly from the polymeric matrix. A larger polymer is therefore preferable to assure favourable controlled release of a larger active ingredient.

Conclusions

Our calculations show how a block copolymer matrix may increase the uptake of a polar active ingredient beyond that for a homopolymer matrix. Linear architectures present some advantages over branched structures: for a given number of nonpolar segments, the active-ingredient relative uptake is larger both in polar and nonpolar solvents. In nonpolar solvents, our results suggest a higher efficiency in microparticle production, whereas in polar solvents, these results suggest an active-ingredient release from the microparticles slower than that from microparticles consisting of branched copolymers. Linear block copolymers appear to provide a promising vehicle for the production of active-ingredient-containing microparticles.

List of symbols

Mc number of polymers in an ensemble

d segment-segment distance

r distance between the center of mass of the polymer and the active ingredient

AI_{ru} active ingredient relative uptake

R_g square root of the sample average radius of gyration squared

$<R_g>$ sample average radius of gyration squared

GREEK

σ diameter of a type-A polymer segment

σ_{ij} size parameter of the interacting segments i and j

$<\rho>$ average active ingredient density in the simulation box

ρ local active ingredient density

ϕ square-well potential

Γ segment density

Acknowledgments

This work was supported by the Director, Office of Science, Office of Basic Energy Sciences, Chemical Science Division of the U.S. Department of Energy under Contract Number DE-AC03-76SF00098. A.S. and N.E. thank the University of Padua, Italy, for a 'Progetto di Ricerca per Giovani Ricercatori' fellowship, and CINECA, under Grant Number 00/598-5, for computing time. D.B. acknowledges support from National Science Foundation.

References

[1] C. Thies, Microencapsulation, in Encyclopedia of Polymer Science Engineering, 2nd Ed., J. Wyley and Sons, 1987.

[2] G. Tse, D. Blankschtein, A. Shefer, S.J. Shefer, Controlled Release 60 (1999), 77.

[3] S.C. Zimmerman, Y. Wang, P. Bharathi, J.S. Moore, J. Am. Chem. Soc. 120 (1998), 2172.

[4] T. Uchida, K. Shiosaki, Y. Nakada, K. Fukada, Y. Eda, S. Tokiyoshi, N. Nagareya, K. Matsuyama, Pharmaceutical Research 15, 11 (1998), 1708.

[5] C. Thomasin, G. Corradin, Y. Men, H.P. Merkle, B.J. Gander Controlled Release 41 (1996), 131.

[6] I. Soriano, M. Llabres, C. Evora Int. Journ. of Pharmaceutics 125 (1995), 223.

[7] C. Witschi, E. Doelker, J. Controlled Release 51 (1998), 327.

[8] E. Walter, K. Moelling, J. Pavlovic, H.P. Merkle J. Controlled Release 61 (1999), 361.

[9] S. Banerjee, R. Premchandran, M. Tata, V.T. John, G.L. McPherson, Ind. Eng. Chem. Res. 35 (1996), 3100.

[10] J. Bleich, B.W. Mueller J. of Microencapsulation 13 (1996), 131.

[11] E. Reverchon J. of Supercritical Fluids 15 (1999), 1-21.

[12] K.F. Pistel, B. Bittner, H. Koll, G. Winter, T. Kissel, J. Controlled Release 59 (1999), 309.

[13] R.F. Barth, D.M. Adams, A.H. Soloway, F. Alam, M.V. Darby Bioconjugate Chem. 5 (1994), 58.

[14] D.A. Tomalia, Scientific American 5 (1995), 62.

[15] I. Gitsov, J.M.J. Frechet, J. Am. Chem. Soc. 118 (1996), 3785.

[16] L. Lue, J.M. Prausnitz, Macromolecules 30, 21 (1997), 6650.

[17] P. Miklis, T. Chagin, A. Goddard III, J. Am. Chem. Soc. 119, 32 (19997), 7458-7462.

[18] M.P. Allen, D.J. Tildesley. Computer Simulation of Liquids, Oxford Science Publications, Claredon Press, Oxford, 1987.

[19] K. Kremer, K. Binder, Computer Physics Reports, 7 (1988), 259.

[20] F.A. Escobedo, J.J. de Pablo, J. Chem. Phys. 104 (1996), 4788-4801.

[21] P.Q. Higgs, H. Orland, J. Chem. Phys, 95, 6 (1991), 4506.

[22] D. Bratko, A.K. Chakraborty, E.I. Shakhnovich, Phys. Rev. Letters 76 (1996), 1844, and J. Chem. Phys. 106, 3 (1997), 1264.

[23] D. Bratko, A.K. Chakraborty, in preparation.

[24] W.G. McMillan, J.E. Mayer, J. of Chemical Physics, 13, 7 (1945), 276.

[25] K. Freed, Renormalization group theory of macromolecules, Wiley, N.Y. 1987.

[26] T. Hino, J.M. Prausnitz, Fluid Phase Equilibria 138 (1997), 105.

[27] L.J. Flory: Principles of polymer chemistry, Cornell University Press, Ithaca and London, 1953.

[28] J. Dautenhahn, C.K. Hall, Macromolecules 27 (1994), 5399.

[29] D. Chandler Introduction to Modern Statistical Mechanics, Oxford University Press, Inc., New York 1987.

[30] S.A. Kuzdzal, C.A. Monnig, G.R. Newkome, C.N. Moorefield, J. Am. Chem. Soc. 119 (1997), 2255.

Table 1 Diameters and well depths used to represent polar and nonpolar solvent conditions. The diameter is reduced by σ, diameter of a type-A segment. Polymer segments are polar (A), partially apolar (B) or apolar (C). Active ingredients of two different sizes are considered (AI1 and AI2)

Species	Diameter	$\frac{\varepsilon}{k_B \cdot T}$ polar solvent conditions	$\frac{\varepsilon}{k_B \cdot T}$ nonpolar solvent conditions
Segment A	1.00	0.15	0.40
Segment B	1.17	0.35	0.30
Segment C	1.23	0.45	0.20
AI1	1.80	0.20	0.35
AI2	2.30	0.20	0.35

Table 2 Active-ingredient relative uptakes, AI_{ru}, and sample average radii of gyration squared, $\langle R_g^2 \rangle$, for different polymers at nonpolar-solvent conditions. The radii of gyration squared are reduced by the diameter of a type-A segment. AI1 and AI2 refer to active ingredients.

Polymer	Type-A Segments	Type-B Segments	Type-C Segments	$AI1_{ru}$	$AI2_{ru}$	$\langle R_g^2 \rangle$
DENDS	21	0	0	0.49±0.01	0.25±0.01	3.65±0.05
DENDS	21	0	4	0.72±0.02	-	4.60±0.05
DENDS	21	4	8	0.96±0.02	0.94±0.04	6.45±0.05
DENDS	21	12	8	1.05±0.02	1.13±0.01	8.0±0.1
DENDS	21	20	8	1.08±0.02	-	9.55±0.2
DENDL	21	2	2	1.19±0.02	-	6.70±0.05
DENDL	21	2	4	1.20±0.02	-	7.4±0.2
DENDL	21	6	4	1.22±0.01	-	8.5±0.3
DENDL	21	10	4	1.23±0.01	-	9.8±0.2
DENDL	21	18	4	1.25±0.01	-	12.1±0.2
LBC	21	0	0	1.10±0.02	1.30±0.01	5.3±0.1
LBC	21	0	1	1.135±0.01	-	5.7±0.1
LBC	21	2	1	1.165±0.01	-	6.4±0.1
LBC	21	5	1	1.22±0.02	1.37±0.02	7.6±0.1
LBC	21	10	1	1.28±0.01	1.46±0.02	9.9±0.2
LBC	21	15	1	-	1.465±0.01	12.4±0.3
LBC	21	16	1	1.285±0.01	-	12.9±0.3

ru = relative uptake

Table 3 Active-ingredient relative uptakes, AI_{ru}, and sample average radii of gyration squared, $<R_g^2>$, for different polymers at polar-solvent conditions. The radii of gyration are reduced by the diameter of a type-A segment. AI1 and AI2 refer to active ingredients.

Polymer	Type-A Segments	Type-B Segments	Type-C Segments	$AI1_{ru}$	$AI2_{ru}$	$<R_g^2>$
DENDS	21	0	0	0.27±0.02	0.11±0.05	4.25±0.05
DENDS	21	12	8	0.635±0.01	0.56±0.01	9.15±0.1
LBC	21	0	0	0.72±0.02	0.60±0.01	6.9±0.1
LBC	21	16	1	0.98±0.01	0.96±0.01	15.3±0.1

ru = relative uptake

Figure captions

Fig. 1 Polymer architectures considered in this work: (1a) linear block copolymer (LBC); (1b) branched copolymer with a linear core (DENDL); (1c) branched copolymer with a 4-arm star core (DENDS). Black segments are polar (type A), white are partially nonpolar (type B), and gray segments are nonpolar (type C). Table 1 shows energetic and size parameters of different segments.

Fig. 2 Segment density, Γ, around the center of mass for a DENDS polymer at nonpolar-solvent conditions. The polymer contains 21 type-A segments, 4 type-B segments, and 8 type-C segments. The dotted line represents segment density upon completion of the core; the dot-line-dot line represents segment density upon completion of the intermediate shell; the continuous line represents segment density upon completion of the entire polymer.

Fig. 3 Radial distribution function for AI2 as a function of the distance from the center of mass of the polymer. The active ingredient is in solution with LBC polymers at nonpolar-solvent conditions. Continuous line stands for a LBC polymer made by 21 type-A segments; dotted line for a LBC polymer made by 21 type-A, 5 type-B, and 1 type-C segments; broken line stands for a LBC polymer made by 21 type-A, 15 type-B and 1 type-C segments (see Table 2 for details). Distance, r', is reduced by the radius of gyration of the polymer.

Fig. 4 Radial distribution function for AI2 as a function of distance from the center of mass of the polymer. The active ingredient is in solution with DENDS polymers at nonpolar-solvent conditions. Continuous line stands for a DENDS polymer made by 21 type-A segments; dotted line for a DENDS polymer made by 21 type-A, 4 type-B, and 8 type-C segments; broken line stands for a DENDS polymer made by 21 type-A, 12 type-B

and 8 type-C segments (see Table 2 for details). Distance, *r'*, is reduced by the radius of gyration of the polymer.

1a:

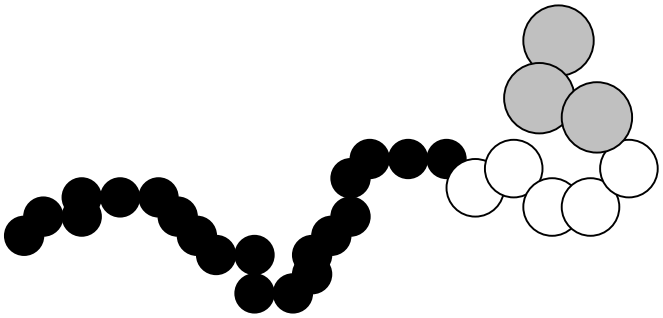

1b:

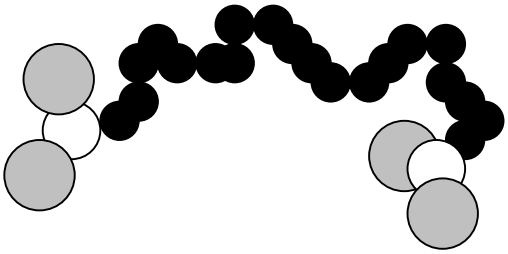

1c:

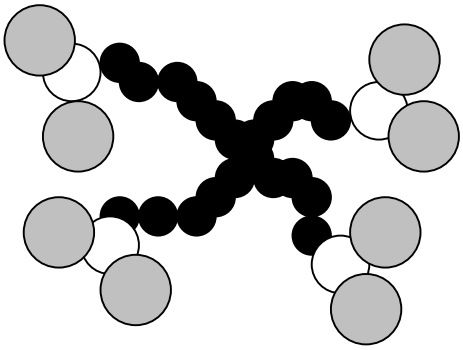

Fig. 1: Striolo et al., Influence of Polymer Structure upon Active-Ingredient Loading….
May 8th, 2000.

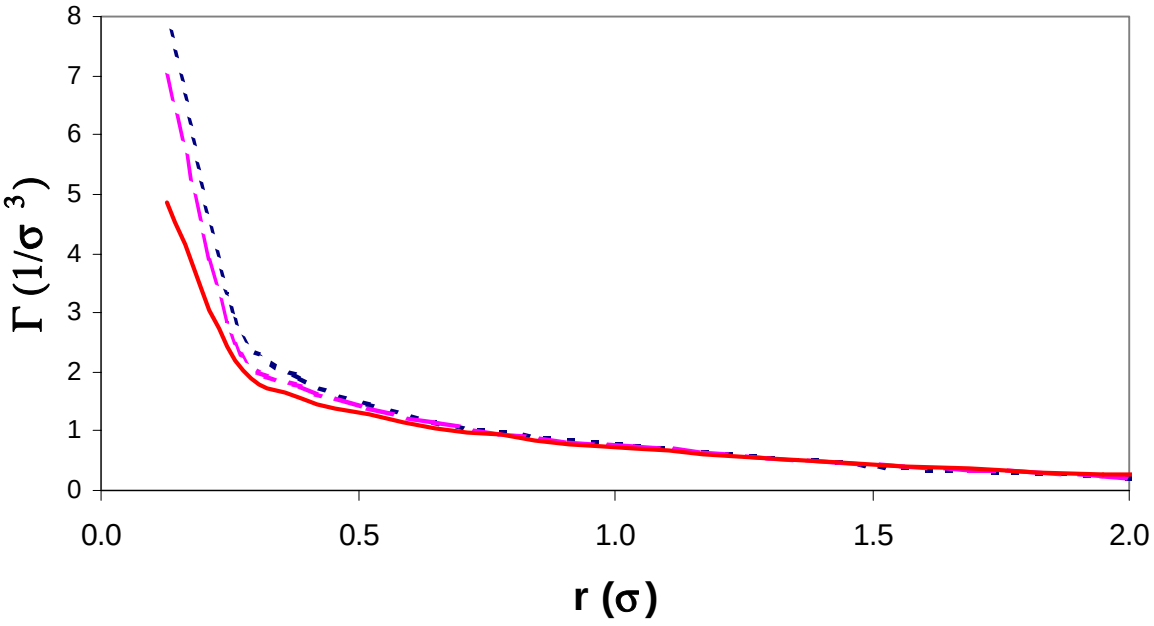

Fig. 2: Striolo et al., Influence of Polymer Structure upon Active-Ingredient Loading….
May 8th, 2000.

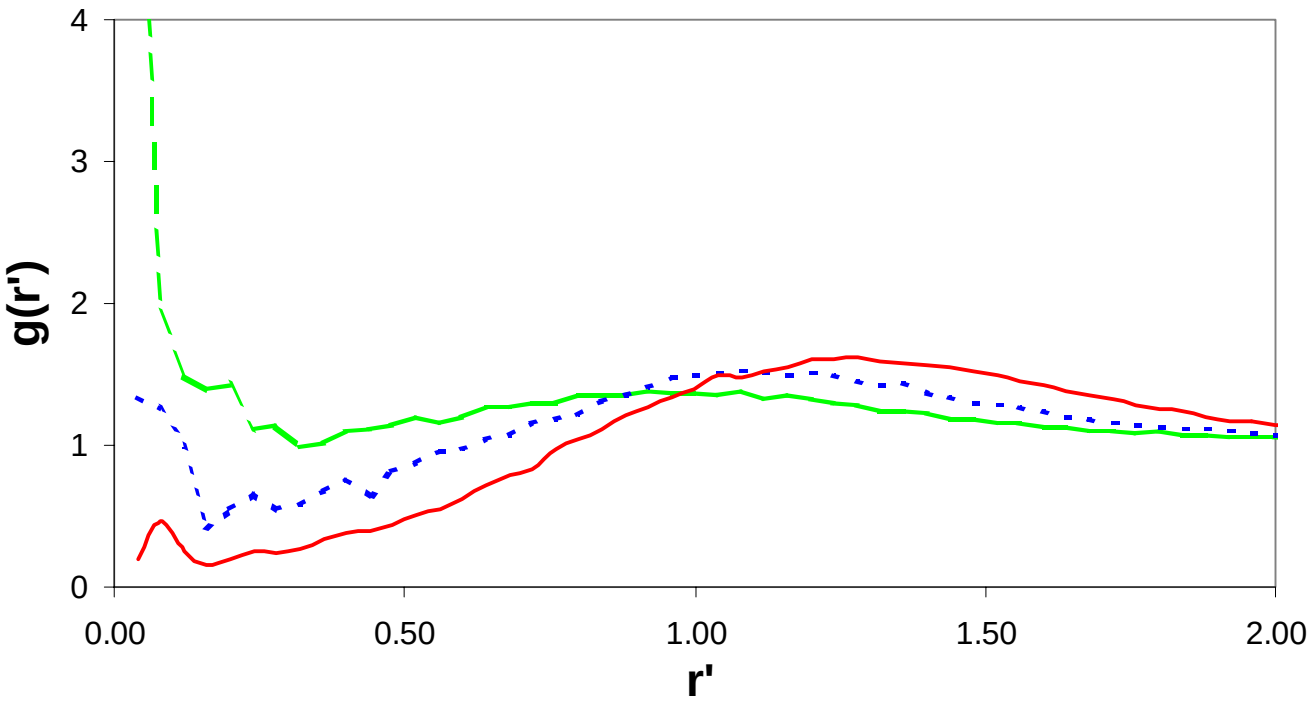

Fig. 3: Striolo et al., Influence of Polymer Structure upon Active-Ingredient Loading….
May 8th, 2000.

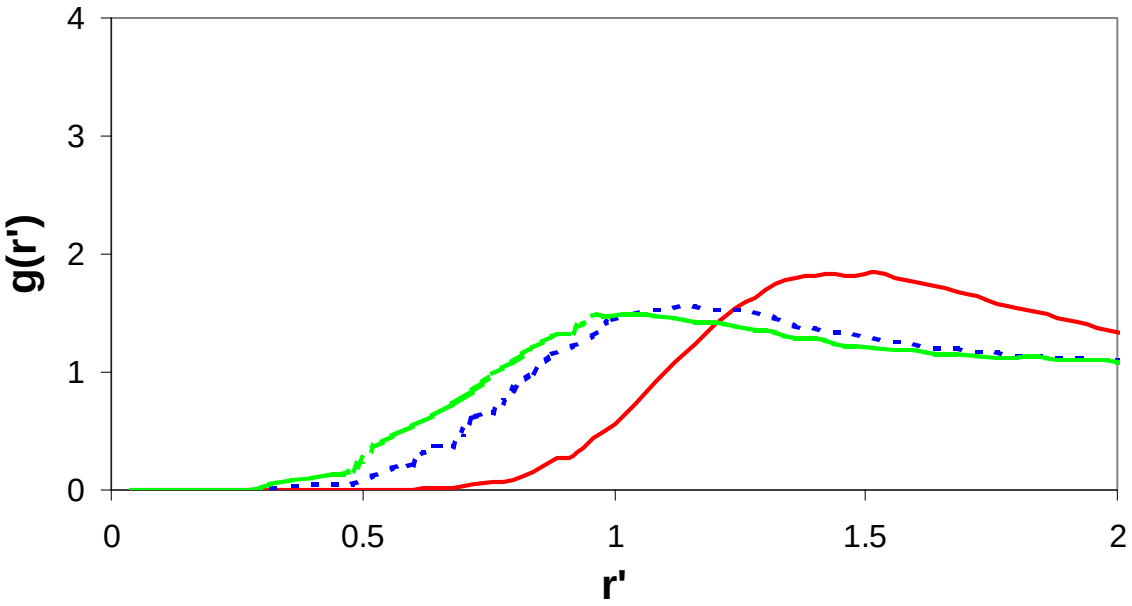

Fig. 4: Striolo et al., Influence of Polymer Structure upon Active-Ingredient Loading….
May 8th, 2000.